AIAA JOURNAL
Vol. 49, No. 7, July 2011

Experimental Investigations on Transpiration Cooling for Scramjet Applications Using Different Coolants

Tobias Langener* and Jens von Wolfersdorf†
University of Stuttgart, 70569 Stuttgart, Germany
and
Johan Steelant‡
ESA, 2200 AG Noordwijk, The Netherlands

DOI: 10.2514/1.J050698

The extremely high heat loads within a scramjet combustor require the use of high-temperature materials combined with efficient cooling concepts. A promising technique is the application of transpiration cooling to ceramic matrix composite materials. A supersonic hot-gas-flow test facility is used to investigate this cooling method. The carbon/carbon samples tested have porosities of about $\varepsilon = 11\%$. The airflow is electrically heated up to 1120 K total temperature with a total pressure of ≈ 3 bar and is accelerated to a Mach number of 2.1 within the test channel. Air, argon, and helium are used as coolants for blowing ratios from 0 to 1%. The surface temperature of the porous wall is measured via thermocouples and infrared thermography. Pressure and mass-flow measurements are used to analyze the throughflow characteristics of the porous materials at various temperature conditions. An approach based upon simplified analytical models is presented to analyze the experimental data of throughflow behavior and cooling efficiency. The simplified thermal model is used to analyze the effect of fluid property variations with temperature on pressure loss for different coolants and shows good agreement with the experimental data.

Nomenclature

A	=	area, m^2
a	=	model constant
b	=	temperature difference, K
d	=	hydraulic diameter, m
F	=	blowing ratio
h	=	heat transfer coefficient, W/m^2 K
I	=	radiation intensity, W/m^2
K	=	permeability, m^2, m
k	=	thermal conductivity, W/m K
L	=	sample thickness, m
l	=	downstream sample position, origin at Laval nozzle throat, m
$\dot{m}$	=	mass-flow rate, kg/s
n	=	exponent in viscosity law
Pr	=	Prandtl number
p	=	pressure, Pa
Re	=	Reynolds number
St	=	Stanton number
T	=	temperature, K
u, v	=	velocity, m/s
V	=	volume, m^3
x, y	=	Cartesian coordinates, m
ε	=	porosity
Θ	=	cooling efficiency
ϑ	=	nondimensional temperature
μ	=	dynamic viscosity, kg/m s
ρ	=	density, kg/m^3

Subscripts

c	=	coolant
cu	=	copper
D	=	Darcian permeability
d	=	based on hydraulic diameter
ex	=	exit of porous wall
F	=	Forchheimer permeability
g	=	hot-gas channel
in	=	inlet
r	=	recovery
ref	=	reference
TC	=	thermocouple
w	=	wall
0	=	without blowing, uncooled

Received 1 June 2010; revision received 20 December 2010; accepted for publication 1 March 2011.

*Research Associate, Institute of Aerospace Thermodynamics, Pfaffenwaldring 31; tobias.langener@esa.int. Student Member AIAA (Corresponding Author).
†Professor, Institute of Aerospace Thermodynamics, Pfaffenwaldring 31.
‡Senior Research Engineer, Aerothermodynamics and Propulsion Analysis Section, Keplerlaan 1. Member AIAA.

I. Introduction

WHEN striving for means of transportation at high supersonic or hypersonic speeds, either for space travel or for commercial aviation, one has to overcome many challenges [1]. In addition to new propulsion concepts, the integration of the vehicle components, and aerodynamic optimization, one of the most important challenges is the exposure of some aircraft components to extremely high aerothermal loads (5 MW/m^2 or more than 3000 K wall temperature possible at a flight Mach number of 8 [1]). These loads are especially apparent at the nose, in the leading-edge region of the plane's wings, and within the propulsion systems. Here, classical materials like metals or simple ceramics can no longer be used because they would thermally and structurally fail. Hence, one is forced to replace these with high-temperature, lightweight components, some of them with active cooling [2]. In this context new porous materials offer very efficient cooling mechanisms such as transpiration cooling and internal cooling within the structure itself. Those materials have to be tested and qualified.

When applying transpiration cooling to a porous wall, a coolant film forms over the surface thickening the boundary layer and therefore reducing the temperature gradients at the wall. This will lead to significantly lower wall heat flux. Because of multiple cooling channels with micrometer dimensions within the porous material, there is also an efficient heat exchange mechanism between the

coolant and the structure. This removes a substantial amount of heat from the ceramic matrix composite (CMC) back into the main flow.

With the test facility available at the Institute of Aerospace Thermodynamics (ITLR) of the University of Stuttgart, it is possible to model operational modes of a ramjet and scramjet combustor at a flight Mach number of 5–6 at an altitude of ≈32 km. In the hot-gas experiments with carbon/carbon (C/C) as the transpiration-cooled CMC material, total temperatures up to $T_{t,g} = 1060$ K at a main-flow Mach number of $M = 2.1$ were set at moderate total-pressure levels of $p_{t,g} = 0.3$ MPa. The cooling efficiency of C/C material with randomly oriented fibers and porosities ($\varepsilon = V_{\text{void}}/V$) of 10.7 and 11.0% was assessed with gaseous air, argon, and helium as coolants. During the experiments, the steady-state surface temperature was measured with thermocouples and infrared thermography and evaluated versus the coolant mass-flow rate. Furthermore, the pressure drop over the porous sample was measured and evaluated.

It was observed, that for the investigated materials and gases, the specific heat of the coolant is a dominating factor for the transpiration-cooling efficiency. The sample's thickness and the test total temperature has less influence on the cooling efficiency. A simple heat-balance model was developed to assess the heat-loss effects in the experimental setup and point out the influence of the gases' specific heat capacity. The model described in Kays et al. [3] proved to be able to predict the heat flux to the porous wall in our setup. Additionally, the effect of the sample's temperature level on its throughflow behavior was addressed by modifying the commonly used Darcy–Forchheimer equation [4]. A higher temperature level leads to higher pressure losses, due to locally higher coolant viscosity and velocity compared with isothermal conditions at the same coolant mass-flow rates.

First, an overview of the state of technology is given. Then the experimental facility is described, followed by the sample integration concept. Next, the measurement system is explained, followed by the throughflow results and a model for the pressure loss. The surface temperature measurements were performed using several thermocouples to obtain the averaged cooling effectiveness as well as infrared thermography for local temperature distributions, which can be used for the development of numerical modeling approaches (see, for example, Langener et at. [5] or Cheuret et al. [6]) Afterward, the surface temperature distribution of the porous sample at varying blowing conditions and a comparison with the simple heat-balance model is shown. Finally, this model is coupled with the model for the throughflow behavior in order to predict the pressure drop of nonisothermal C/C material.

II. Transpiration-Cooling Studies: An Overview

The first studies on transpiration cooling for aerospace application were carried out in the late 1940s. Rannie [7] developed an analytical approach for the porous-wall temperature by looking at the laminar, transpired sublayer and compared his theory to experiments. It only fits well for porous substrates of low thermal conductivity, due to lateral heat conduction in the samples. Eckert and Livingood [8] showed in an analytical study the superiority of this cooling technique versus purely convectively cooled and film-cooled walls. The investigated Reynolds number range with respect to the length of the flat plate for turbulent flows was from $Re_g = 10^5, \ldots, 10^9$ and blowing ratios $F = (\rho_c v_c)/(\rho_g u_g)$ up to 0.012, which is a similar regime to that studied in this paper. For the hot-gas-side heat transfer a Stanton number relationship between the case of transpiration cooling and uncooled wall ($St_g/St_{g,0} = (F/St_{g,0})/(e^{F/St_{g,0}} - 1)$) was given. Thereby, thermal equilibrium between the porous wall and the transpiration coolant was assumed and radiation from the surroundings to the wall was neglected. The higher effectiveness of transpiration cooling was again proven in 1970 by Laganelli [9], who compared this technique to more advanced prediction methods for film or effusion cooling.

During the 1950s fundamental analytical [10] and experimental [11,12] studies were carried out, to investigate and prove the known relationships for the Stanton number and the friction coefficient in the case of transpired boundary layers. Detailed experimental studies on an isothermal porous wall with transpiration were carried out by Moffat and Kays [13] and Simpson et al. [14]. These studies proved the equation for $St_g/St_{g,0}$ given by Eckert and Livingood [8] in a hot-gas Reynolds number range of $Re_g = 10^5 - 2 \cdot 10^6$ and with blowing ratios up to $F = 0.0096$. Generally, it was reported that small blowing ratios of $F < 0.01$ are sufficient for any cooling application [7,15,16], which was also observed during this study.

Later, it was shown that a porous wall can have a thermal effectiveness smaller than unity [17], which means no thermal equilibrium between wall and coolant. In this case the coolant exits the wall at a lower temperature and is able to pick up more heat from the main flow close to the wall. This leads to lower heat transfer coefficients for structures that are imperfect heat exchangers, which was expressed by a correction factor [17].

To demonstrate the use of transpiration cooling for potential supersonic application, in 1955 Chauvin and Carter [18] carried out a study with a transpiration-cooled cone in a $M = 2.05$ freestream at sea-level conditions. Nitrogen, helium, and liquid water were used as coolants. Liquid water showed the best cooling performance, due to its evaporation enthalpy, whereas the surface temperature reduction using helium was three times higher than with nitrogen. This influence was also shown by Laganelli [9]. The impact of the coolants' specific heat capacity, for example, has been described by Kays et al. [3]. Bartle and Leadon [19] conducted an experimental study with a $M = 3.2$ freestream flow on a flat plate, reporting only a minor influence of Re_g on the wall temperature when using transpiration cooling. In 1966 Woodruff and Lorenz [20] presented a study in which foreign gas injection into a hypersonic boundary layer was investigated, confirming previous studies [10,19]. These effects of freestream Mach number and specific heat of the coolant were shown analytically as well [21].

More recent studies of transpiration cooling with foreign gas injection were presented by Meinert et al. [22]. The results were compared with a modified Rannie equation and compared with real application in a high-pressure hydrogen combustion environment similar to the experiments presented by Serbest [23].

With the availability of lightweight ceramic matrix composites such as carbon/carbon (C/C) [24] or silicon-carbide-infiltrated carbon fibers (C/C-SiC) [25], transpiration cooling now seems to be a promising technique for combustion-chamber cooling for high-speed aerospace applications. Here, continuous heat loads of up to 17 MW/m^2 can appear, where regeneratively cooled walls cannot be used anymore [26,27]. The porous nature of these materials combined with the insensitivity to thermal shocks and thermal expansion and their high maximum service temperatures of up to $T_{w,\max} = 1800$ K [28] make them ideal candidates for application in supersonic hot-gas environments. System studies showed that using transpiration cooling in rocket thrust chambers yields much better performance than regeneratively cooled systems [15,16]. Therefore, recent investigations using C/C combustor liners in model rocket combustion chambers were pursued. Serbest et al. [29] conducted basic hydrogen/oxygen combustion experiments using transpiration cooling. They found a good resistivity of the material with respect to damage and erosion. Several tests concerning transpiration cooling and the throughflow behavior were summarized by Hald et al. [30]. For higher combustion-chamber pressure regimes up to $p_{t,g} = 8$ MPa the transpiration-cooled C/C materials with gaseous hydrogen as coolant worked without major damages. An experimental study using air transpiration cooling with C/C for scramjet or ramjet combustion-chamber applications was carried out by Langener et al. [31]. The main-flow total temperature ranged up to $T_{t,g} = 750$ K and the surface temperature of several flat-plate C/C samples exposed to heated subsonic or supersonic was measured for different blowing ratios. The coolant mass-flow rate was shown to be the most influential parameter on the cooling efficiency compared with the hot-gas Mach number, Reynolds number, and sample porosity within the investigated range.

With respect to the above mentioned studies the work described in this paper is meant to show the validity of previous models with respect to the less investigated and newer CMC wall material. Most

of the studies using this material were related closer to real application, which hardened the detailed qualification of the cooling mechanisms. Furthermore, the heat conduction effects during the transpiration-cooling tests in a nonadiabatic test setup that was already pointed out by Rannie [7] could be analyzed and described by extending the model for foreign gas injection transpiration cooling given by Kays et al. [3]. This thermal model is applied to consider the temperature dependency of the fluid viscosity with respect to the throughflow and, therefore, pressure-loss characteristics. The obtained extended Darcy–Forchheimer equation showed good agreement with the experimental data for different thermal loads and coolants.

III. Experimental Procedure

A. Test Facility

The experimental facility used is dedicated to supersonic combustion experiments as described, for example, by Scheuermann et al. [32] or Vellaramkalayil et al. [33]. In this study, it was modified and extended to accommodate the transpiration-cooling tests. Figure 1 shows the test-bench schematic. The upper portion displays the coolant distribution system, and the lower part shows the main flowpath.

The air for the main flow is compressed by a staged screw compressor driven by an electrical motor that can deliver flows at 1.05 MPa nominal total pressure and up to 1.45 kg/s of the main mass-flow rate. Additionally, it is possible to use a pebble-bed air dehumidifier in order to obtain dry air with a relative humidity in the order of 0.1% with respect to the compressed volume-flow rate. After the screw compressor, two electrical heaters are installed that are capable of heating the flow convectively using resistively heated metal rods up to 1450 K total temperature. During the tests described in this paper the maximum investigated total temperature was $T_{t,g} = 1120$ K. Directly after the heaters the hot-gas plenum can be found. The test section is bolted in at this location. Here, total temperature $T_{t,g}$ (accuracy of 1.1 K) and total pressure $p_{t,g}$ (accuracy 0.008 MPa) are measured and used for determining the flow conditions within the test section. The main volume-flow rate is measured by an Endress+Hauser Prowirl PW73 vortex flow meter with an uncertainty of 0.001 m^3/s upstream of the heaters. OMEGA pressure (0.008 MPa accuracy) and temperature (type-K thermocouple, accuracy of 1.1 K) transducers are installed at the same location to determine the mass-flow rate.

The coolant air is provided by four pressure tanks of 2 m^3 volume each, which are pressurized at 10 MPa and additionally serve as an emergency supply for the electrical heaters in the case of a screw compressor malfunction. In the test chamber the coolant supply pressure is decreased to 1.5 MPa by a pressure reducer and the coolant mass-flow rate is determined and set by a Teledyne-Hastings HFC-303 thermal mass-flow controller (accuracy 4.8×10^{-5} kg/s), which can measure flows up to 0.0108 kg/s. Argon and helium are provided by compressed gas bundles and the mass-flow rate is set and determined by the same controller as for air using conversion factors.

B. Test Section

The test section itself (see schematic in Fig. 2a) is a 1.258-m-long, water-cooled copper channel with multiple openings for optical

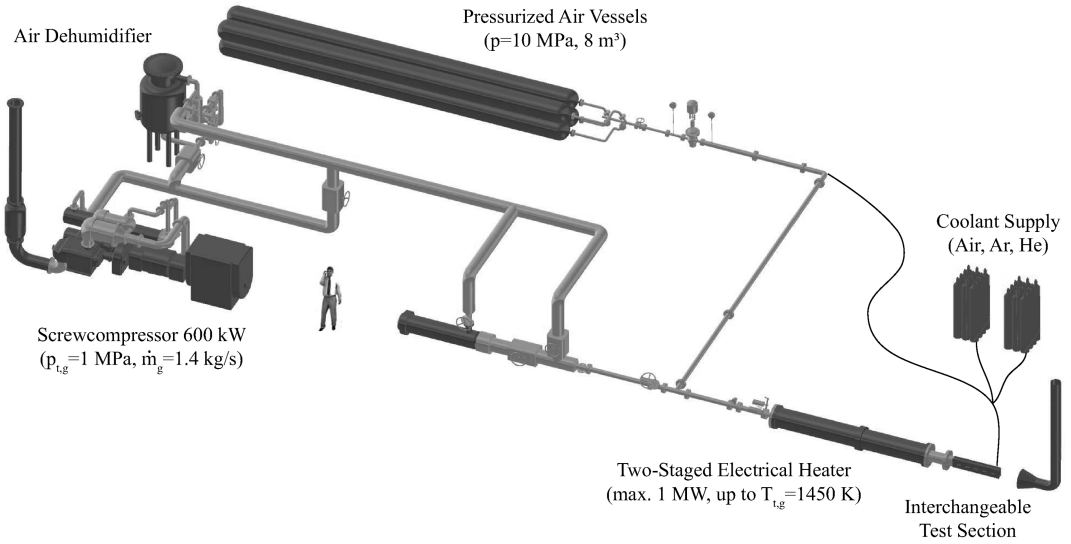

Fig. 1 ITLR supersonic combustion and hot-gas-flow test bench.

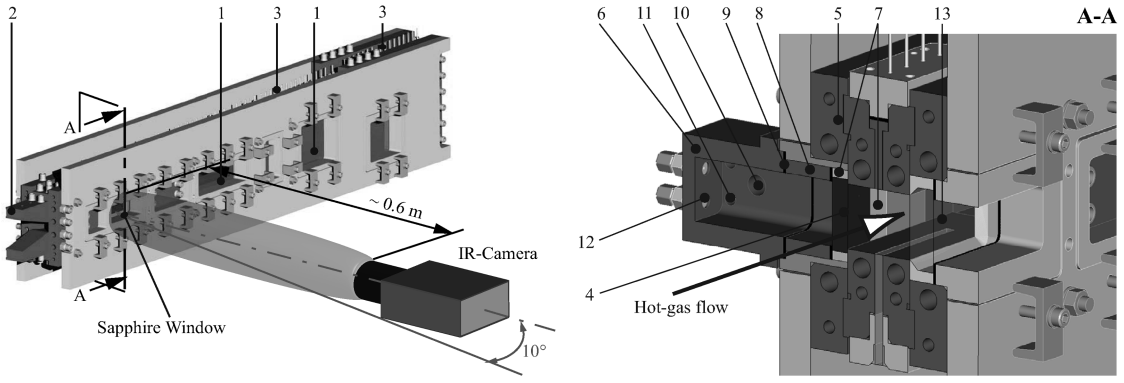

a) Test section with IR-thermography-setup **b) Sample integration concept**

Fig. 2 Experimental setup.

access (label 1 in Fig. 2a). The flow enters the channel through a Laval nozzle (label 2), that expands the air to $M = 2.1$ with the given nozzle contour. The static pressure can be measured with an accuracy of 100 Pa along the main stream coordinate at 71 positions (label 3), which are continuously monitored during the experiments. The height of the test section is 35.4 mm and the width is 40 mm leading to a copper-channel cross-sectional area of 0.001416 m^2. The optical setup for the infrared (IR) measurements is schematically displayed in Fig. 2a. The surface temperature of the porous-wall segment can be monitored through a sapphire window on the opposite wall.

The sample integration concept is shown in Fig. 2b. The porous sample (label 4 in Fig. 2b) is directly bearing on the water-cooled copper parts (label 5) of the test channel and clamped by the coolant plenum (label 6) from the back. It is embedded for insulation purposes into a Macor frame (label 7) and held back by a spacer (label 8). Carbon sealings (label 9) are put between the sample, spacer, and coolant plenum. At the plenum, the coolant is supplied from the side (label 10). Its pressure and temperature (label 11) are measured at the same position. From the top, 4 K-type thermocouples (OMEGA SuperOMEGACLAD^{TM}, 1.2 K accuracy) are led through the plenum (label 12) into the sample, where they are installed tightly and flush with the porous wall's surface. For this, the tips of the thermocouples were coated with a thin layer of LOCTITE 5399 sealant. The holes were drilled at a 1.1 mm diameter, except from approximately 2 mm below the hot-gas surface, where a 1.0 mm hole was manufactured. This ensured the leak tightness and firm positioning of the thermocouple shaft, which was slightly larger in diameter than 1.0 mm. Immediately afterward, the tip of the thermocouple was adjusted with a flat tool from the hot-gas side of the porous wall to guarantee the flush installation with the sample surface and prevented it to measure the flow boundary layer temperature. A sketch of the sample with its bore hole pattern is given in Fig. 3. The data were read by an Agilent 34970A data logger and displayed and evaluated via a LabVIEW 8.5 software routine. The sapphire window (label 13) was also insulated by a Macor frame from the water-cooled copper walls.

C. Infrared Thermography System

In addition to the thermocouple measurements, infrared thermography was used to obtain a 2-D surface temperature map of the porous material. A Mitsubishi IR-M700 thermal imager (wavelength range of 1.2–5.9 μm) was used and the data were recorded by the IRBIS 3.0 Software by Infratec, GmbH. The resolution of the camera was 720×480 pixels, leading to an optical resolution of approximately 10 pixels/mm for this setup. Within the setup unknown optical quantities appear such as the object's emissivity, reflected radiation, and temperature of the optical path. Therefore, the IR data were in situ calibrated [34–36] using the thermocouple data T_{TC} for the whole set of coolant mass-flow rates ($F = 0$ up to F_{max}) to address the relevant temperature range. The local radiation data I_{cam} around the thermocouple positions was averaged from every steady-state image. These data pairs can be fitted against a function similar to Planck's law:

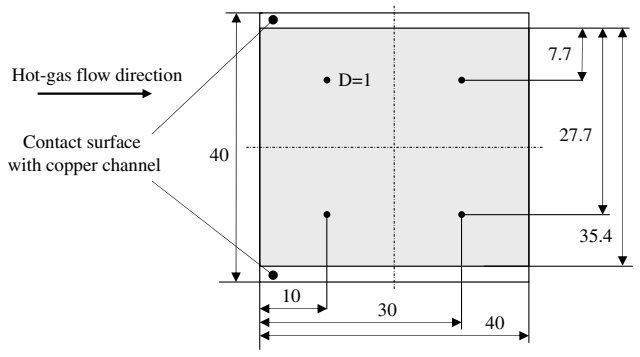

Fig. 3 Sketch of the porous-wall sample geometry with its bore hole pattern.

Table 1 Estimated uncertainties in hot-gas experiments

Name	Symbol x_i	Uncertainty δx_i
Blowing ratio	F	2–16%
Cooling efficiency	Θ	1–15%
Throughflow velocity	v	1–10%
Pressure drop per unit length	$\Delta p/L$	1–3%

$$I_{cam} = \frac{R}{e^{B/T_{TC}} - F} \tag{1}$$

where R, B, and F are calibration constants and the result of the fitting routine. Knowing these parameters, the 2-D temperature maps can be calculated from the 2-D infrared data. Brauckmann [37] presented a study on in situ calibrated infrared data in the field of gas turbine film-cooling research reporting an uncertainty in the object temperature of $\delta T_w = 4$ K after calibration.

D. Experimental Uncertainty

Following the uncertainty analysis for single sample experiments [38,39], the accuracy for the computed experimental parameters could be estimated with a confidence interval of 95%. The uncertainty margin of the most important experimental parameters is given in Table 1. The blowing ratio F is a variable that is computed from several measured variables; therefore, the uncertainty can be up to 16% for the lowest blowing ratios, due to the accuracy of the mass-flow meter. The same applies for the superficial throughflow velocity v. The cooling efficiency given in the results is computed with an average of the four installed surface thermocouples.

E. Investigated Material

Two different C/C samples manufactured by the DLR, German Aerospace Center were investigated. They are a product of the second step of the liquid silicon infiltration process to manufacture C/C-SiC [24,25]. The first step is the shaping. Here, carbon-fiber-reinforced plastics are made from precursors, additives, and fibers or prepregs (impregnated fabrics) by various process techniques. In this study, samples manufactured via autoclave technique [24] were used. The second step of processing is pyrolysis, where the resin matrix is changed to carbon. Depending on the resins and the fibers, certain porosities can be achieved. In this study so-called randomly oriented C/C is used. Here, each fabric is rotated by $\pm 15^\circ$ relative to each other. The physical properties of the samples are shown in Table 2. The permeability coefficients were determined by a curve-fitting technique [31]. The values shown in Table 2 are coefficients obtained from cold-flow tests without the mainstream using air. The sample size was 0.04×0.04 m^2, whereas only 0.0354 m of the height were exposed to the main flow. The permeability in the fiber parallel direction was not assessed in this study.

IV. Data Analysis and Results

A. Throughflow Behavior of C/C at Different Test Temperatures

During the hot-gas tests, the coolant supply pressure was measured at equilibrium with respect to the coolant temperature and pressure for every blowing ratio. With the coolant mass-flow rate for a certain blowing ratio the pressure drop can be expressed in terms of throughflow velocity. From these data, the permeability coefficients K_D and K_F can be determined by curve-fitting the Darcy–Forchheimer Eq. (2) to them. In previous studies [31,40,41], the fluid properties were always assumed at isothermal conditions throughout the porous specimen, and the density was considered to be a function of pressure using the perfect gas law:

$$\frac{\Delta p}{L} = \frac{p_{in}^2 - p_{ex}^2}{2 p_{in} L} = \frac{\mu_{in}}{K_D} v_{in} + \frac{\rho_{in}}{K_F} v_{in}^2 \tag{2}$$

In the case of nonisothermal throughflow, which is related to transpiration-cooling applications, the temperature dependency of

Table 2 Properties of the investigated samples

	$L \times 10^3$, m	ε%	$K_D \times 10^{14}$, m^2	$K_F \times 10^8$, m	ρ, kg/m^3	c_p, J/kg K	k, W/m K
Sample 1	10	11	9.07	1.72	1400	1300	14
Sample 2	5	10.7	6.18	3.88	1400	1300	14

Table 3 Reference dynamic viscosity quantities for used coolants (at 300 K)

Coolant	μ_{ref}, kg/(m s)	n
Air	18.38E − 6	0.70
Argon	22.67E − 6	0.77
Helium	19.93E − 6	0.69

the viscosity and the density needs to be considered. The influence of the changes of gas property on the pressure loss over the porous material will not be negligible. This will become of importance during system-level design and for modeling purposes. Therefore, an extended Darcy–Forchheimer equation is derived assuming thermal equilibrium within the sample for a one-dimensional situation. The nondimensional energy equation for this case is given by Eq. (3):

$$\frac{\mathrm{d}\vartheta}{\mathrm{d}X} = \frac{1}{C}\frac{\mathrm{d}^2\vartheta}{\mathrm{d}X^2} \tag{3}$$

where

$$\vartheta = \frac{T - T_{\text{in}}}{T_w - T_{\text{in}}} \qquad X = \frac{x}{L} \qquad C = \frac{\rho c_p v L}{k}$$

At the hot-gas side ($X = 1$) of the porous-wall section a constant temperature ($\vartheta = 1$) is used, which can be later provided by the measurements T_w or separate model predictions. The coolant side ($X = 0$) is assumed to be at coolant inlet temperature ($\vartheta = 0$), leading to the solution:

$$\vartheta = \frac{e^{CX} - 1}{e^C - 1} \tag{4}$$

For the investigated throughflow velocities and the given coolant and sample properties the parameter C is relatively small ($0 \leq C \leq 1.51$). This means that the temperature distribution within the CMC wall can be approximated for simplicity by a linear function:

$$T = T_{\text{in}} + (T_w - T_{\text{in}})\frac{x}{L} = T_{\text{in}} + b\frac{x}{L} \tag{5}$$

Equation (5) is used to locally determine the coolant viscosity incorporating a general power law [Eq. (6)]:

$$\mu = \mu_{\text{ref}}\left(\frac{T}{T_{\text{ref}}}\right)^n = \mu_{\text{ref}}\left(\frac{T_{\text{in}} + b(x/L)}{T_{\text{ref}}}\right)^n \qquad T_{\text{ref}} = 300\ \text{K} \tag{6}$$

For the investigated coolants the reference quantities at 300 K [42], which are used in Eq. (6), are given in Table 3.

The Darcy–Forchheimer equation in differential form can be written as follows [4]:

$$\frac{\mathrm{d}p}{\mathrm{d}x} = -\left(\frac{\mu}{K_D}v + \frac{\rho}{K_F}v^2\right) \tag{7}$$

First, the superficial throughflow velocity $v = \dot{m}_c/\rho A_c$ and the perfect gas law for the density $\rho = p/RT$ are substituted, followed by Eqs. (5) and (6). A_c here depicts the actively cooled surface, or porous flow cross section, which equals 35.4×40 mm for these experiments. After separation of variables, this yields

$$p\,\mathrm{d}p = -R\left\{\frac{\dot{m}_c}{K_D A_c}T_{\text{in}}\mu_{\text{in}}\left(1 + \frac{b}{T_{\text{in}}}\frac{x}{L}\right)^{n+1} + \frac{\dot{m}_c{}^2}{K_F A_c^2}T_{\text{in}}\left(1 + \frac{b}{T_{\text{in}}}\frac{x}{L}\right)\right\}\mathrm{d}x \tag{8}$$

After integration from inlet (in) to outlet (ex) conditions, an extended form of the Darcy–Forchheimer equation with $v_{\text{in}} = \dot{m}_c/\rho_{\text{in}}A_c$ is obtained. The factor b depicts the temperature difference of the coolant between entering and leaving the porous wall. The permeability coefficients (see Table 2) used in this computation were previously determined from the experimental data at ambient conditions with no main flow and air as a test gas:

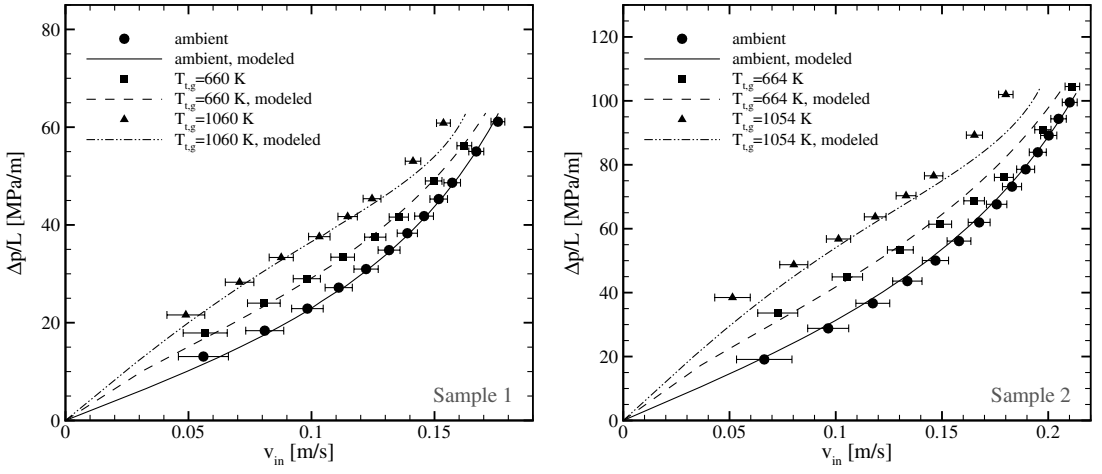

a) Sample 1, Coolant: Air **b) Sample 2, Coolant: Air**

Fig. 4 Normalized pressure loss versus superficial throughflow velocity showing the temperature effect; comparison of throughflow model with experimental data.

$$\frac{p_{\text{in}}^2 - p_{\text{ex}}^2}{2p_{\text{in}}L} = \frac{\mu_{\text{in}}}{K_D} v_{\text{in}} \frac{1}{\frac{b}{T_{\text{in}}}(n+2)} \left[\left(1 + \frac{b}{T_{\text{in}}} \right)^{n+2} - 1 \right] + \frac{\rho_{\text{in}}}{K_F} v_{\text{in}}^2 \left(1 + \frac{b}{2T_{\text{in}}} \right) \tag{9}$$

For isothermal conditions, which means $T_{\text{in}} = T_{\text{ex}}$ or $b = 0$, Eq. (9) collapses into the compressible definition [Eq. (2)]. In Figs. 4a and 4b this analytical approach has been compared with the experimental data. One can see a very good agreement between the predictions from Eq. (9) with the experimental pressure-loss data of both investigated samples at different test temperatures. The data for the throughflow test at ambient conditions with no main flow is shown as circles and a solid line. The biggest impact of the non-isothermal sample conditions can be seen at low or moderate mass-flow rates and throughflow velocities. Here, the pressure drop can be twice as high as compared with the cold-flow tests. For higher coolant mass-flow rate the curves almost collapse again, since the temperature within the sample approaches isothermal conditions at coolant inlet temperature. This is due to the high cooling efficiency of the porous wall at high coolant mass-flow rates (see Sec. IV.C). This shows that the evaluated permeability coefficients from cold-flow experiments can well be used to predict the pressure losses under thermal loadings when taking the temperature dependency of the coolant's properties adequately into account. The presented model has been set up for thermal equilibrium between the coolant and the porous wall and the permeability coefficients are determined separately. Therefore, the porosity of the sample and the pore size will not affect the presented results unless the material is altered significantly such that a different thermal situation presents itself.

B. Surface Temperature Distribution

To get extended information of the thermal behavior of the transpiration-cooled porous C/C wall segment, which means to quantify the influence of the gases' specific heat capacity on the boundary layer and internal heat transfer, experiments with different coolant gases were conducted. In addition to the reference case where air is used as a coolant, we used argon and helium.

In Fig. 5a–5d surface temperature distributions obtained with the infrared camera system are displayed. In Fig. 5a the uncooled case is given. On top and bottom of the sample one can see the influence of the lateral heat conduction due to the water-cooled environment in which the wall segment is embedded. Because of this, the recovery temperature ($T_{\text{rec}} \approx 1011$ K) at the wall is not reached for the case without transpiration. The maximum measured wall temperature was at $T_{w,\max} \approx 670$ K. Additionally, the structure of the C/C is somewhat visible, because of nonuniform optical parameters on the surface and fibers. Also, the tips of the wall thermocouples can be distinguished from the porous wall, due to the differing emission coefficient of their steel sheaths. This also indicates the installation location of the thermocouples on the sample.

With increasing blowing ratio F the surface temperature decreases significantly. Very small blowing ratios of $F = 0.001$, corresponding to 0.1% coolant mass flux in relation to the hot-gas mass flux, lead to a temperature reduction of ≈90 K. For comparison, in Fig. 5c and 5d the surface temperature with foreign gas injection (helium) is given.

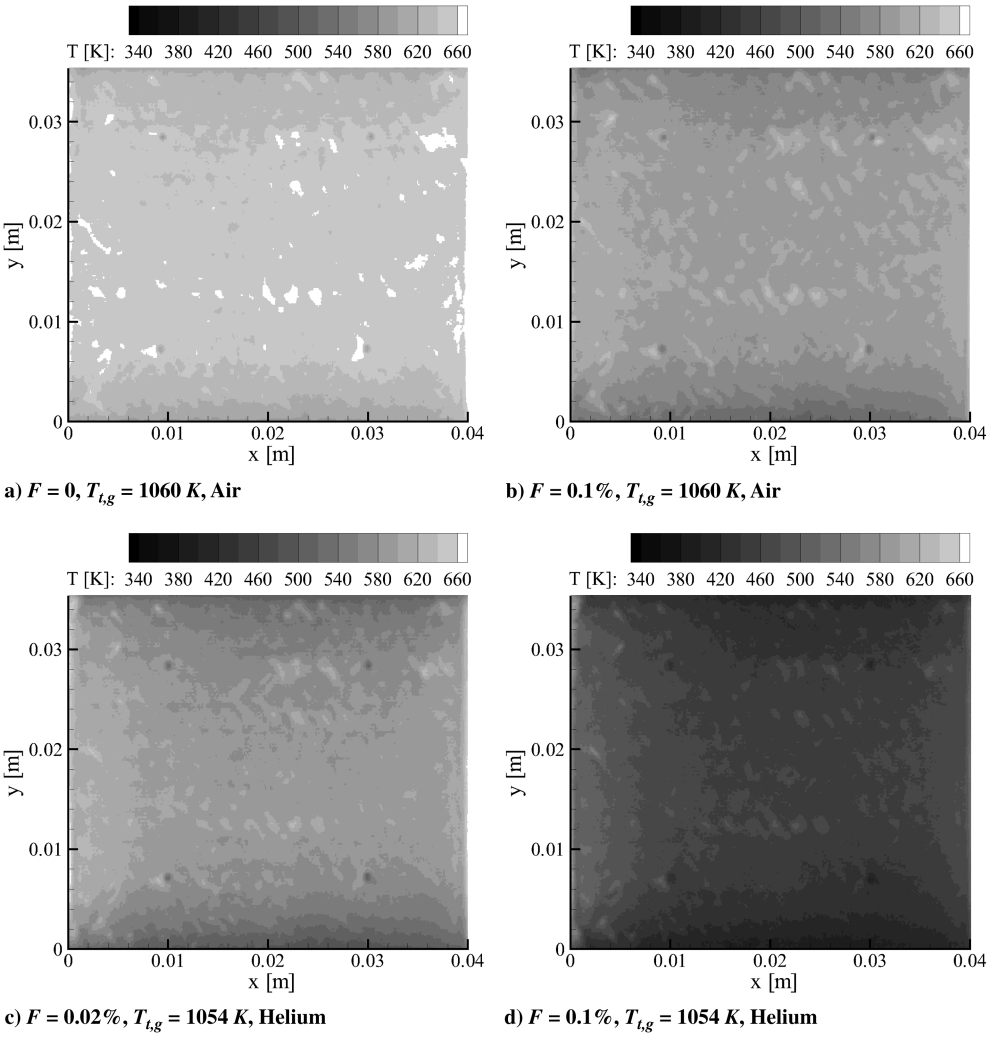

a) $F = 0$, $T_{t,g} = 1060$ K, Air

b) $F = 0.1\%$, $T_{t,g} = 1060$ K, Air

c) $F = 0.02\%$, $T_{t,g} = 1054$ K, Helium

d) $F = 0.1\%$, $T_{t,g} = 1054$ K, Helium

Fig. 5 Surface temperature distributions of C/C sample 1 for different blowing ratios with air as a coolant (top) and helium as a coolant (bottom); main-flow conditions $M_g = 2.1$ and $P_{t,g} = 2.97$ bar.

At a very low blowing ratio of $F = 0.0002$ with helium (Fig. 5c) approximately the surface temperature level obtained at $F = 0.001$ with air as a coolant (Fig. 5b) is reached with helium. The factor of 5 in F for the same wall temperature corresponds roughly to the ratio in specific heat capacity for helium and air. For a higher blowing ratio the surface temperature decreases significantly. From the infrared data, one is able to tell, that transpiration cooling applied to C/C is a very efficient process and that the cooling is nearly homogeneous over the sample's surface. Additionally, it is strongly dependent on the gases' specific heat capacity.

C. Cooling Efficiency

Because of the significant heat conduction effects in the water-cooled test channel described above, which were also described in Langener et al. [31], a nondimensional temperature ratio to describe the cooling efficiency of the transpiration-cooled porous wall is used in this setup. It aims to reduce the influence of the lateral heat conduction effects in such a situation and data interpretation by referring to the non-transpiration-cooled case. It ranges from zero (no transpiration cooling) to unity (complete cooling). With this definition, one is able to compare tests with, for example, different coolants and different sample materials among each other. The wall-temperature data have been averaged from the four wall thermocouples:

$$\Theta = \frac{\bar{T}_{w,0} - \bar{T}_w}{\bar{T}_{w,0} - T_c} \tag{10}$$

In Figure 6a and 6b the cooling efficiency [Eq. (10)] is plotted versus the coolant mass-flow rate per cooled area. On the left-hand side, the influence of the different coolants using sample 1 is shown. The impact of the gases' specific heat capacity is clear. With the same amount of coolant mass-flow rate helium cools the wall segment much better than air, whereas the cooling efficiency with argon is inferior, due to its smaller $c_{p,c}$. Furthermore, the cooling efficiency obtained from the infrared data is given in Fig. 6a as filled symbols. The data for $\bar{T}_{w,0}$ and $\bar{T}_w$ have been obtained in this case by averaging the complete surface area, including the warmer and colder parts of the porous wall, whose absolute difference is one order larger than the measurement uncertainty in the wall temperature, for both infrared data and thermocouple data. The agreement with the thermocouple data (open symbols) is very good, which shows that the thermocouples are installed in locations representing the cooling efficiency for the whole sample.

In the following, only the thermocouple data are used for Θ. The cooling efficiency of sample 2 at different hot-gas total temperature ranging from $T_{t,g} = 400$ up to 1120 K is shown in Fig. 6b. Note that the nondimensional temperature ratio Θ is fairly independent from the hot-gas total temperature at the same Mach number and coolant mass-flow rate. For further evaluation, only the data at a hot-gas total temperature of $T_{t,g} \approx 1060$ K will be discussed.

To investigate the effect of the coolants in more detail, the experimental data were compared with different approaches in literature. All models follow a 1-D heat-balance approach with semi-empirical assumptions for the heat transfer coefficients for the cooled and uncooled cases, neglecting lateral heat conduction. Eckert and Livingood [8] use a correlation for flat-plate heat transfer, and Kays et al. [3] and Rannie [7] use a relationship for fully developed channel flow. In Fig. 7a cooling efficiency predictions using the models of Rannie [7] and Eckert and Livingood [8] are shown. Typically, the model of Rannie [7] overestimates the cooling efficiency measured in our test setup. Eckert and Livingood's [8] model fits well for argon as a coolant, and overestimates Θ for higher coolant $c_{p,c}$ (air and helium). Both approaches incorporate the ratio of specific heat capacities between the main flow and the coolant as a proportional factor.

In Fig. 7b the model of Kays et al. [3] is compared with the experimental data with a hot-gas Stanton number without blowing of $St_{g,0} = 0.0044$. This value has been chosen arbitrarily to achieve an agreement of the curves with the test data and to point out that this model is able to correctly calculate the trend of varying coolant specific heat capacities. For our test setup typical empirical correlations yield much lower $St_{g,0}$ than used in Fig. 7b. Because of its good agreement with the test data with respect to the foreign gas effect, the Kays et al. model was chosen for a modified approach to compensate for the lateral heat conduction appearing in our setup.

To capture this effect, we set up a simplified heat balance for the given test arrangement in Eq. (11). It contains the convective heat transfer onto the porous wall, the heat picked up by the coolant within the wall and the heat conduction losses toward the water-cooled copper parts of the test channel at a temperature of T_{cu}. The heat conduction term leads to less heat that has to be removed by the transpiration-cooling mechanisms (internal and external). Therefore, the cooling efficiency will be lower, when including lateral heat conduction in our model. Additionally, thermal equilibrium between the coolant and the porous wall and no coolant side heat transfer has been considered:

$$\underbrace{h_g(T_{r,g} - T_w)}_{\text{convective heat transfer}} = \underbrace{\rho_c c_{p,c} v_c (T_w - T_c)}_{\text{internal cooling}} + \underbrace{B(T_w - T_{\mathrm{cu}})}_{\text{heat conduction losses}} \tag{11}$$

The coefficient B accounts for the thermal resistance from the porous surface to the water-cooled copper parts in steady state. It is assumed to be constant for all blowing ratios. B can be determined from a heat balance of the uncooled case, where the heat convected onto the wall is only laterally conducted into the copper parts:

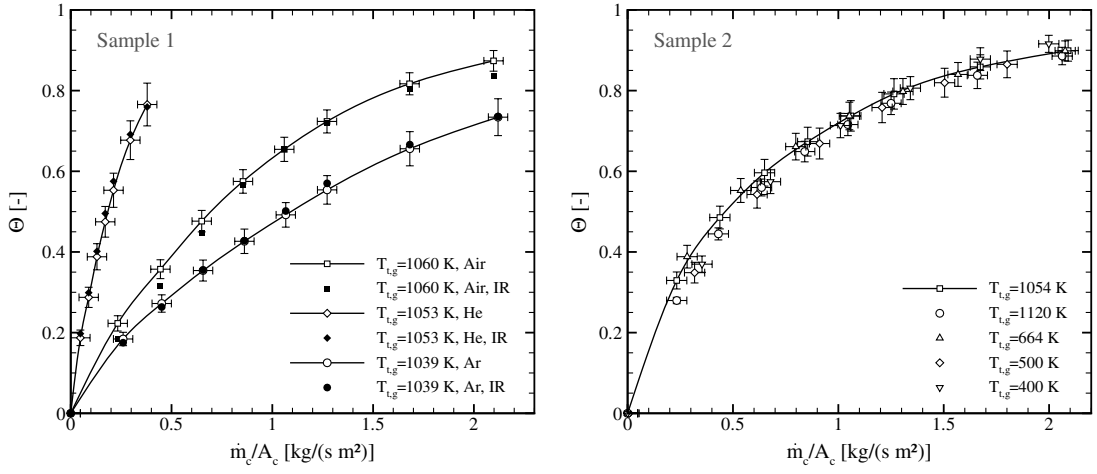

a) Sample 1: Different coolant gases. Comparison of thermocouple to infrared data

b) Sample 2: Different total temperatures for air as a coolant

Fig. 6 Nondimensional temperature versus coolant mass flux $\dot{m}_c/A_c$.

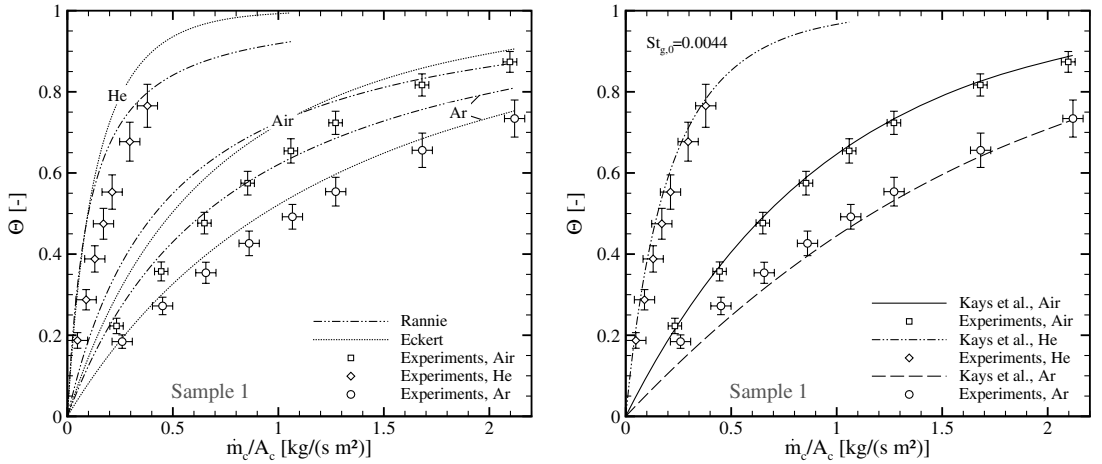

a) Models of Rannie [7] and Eckert and Livingood [8] **b) Model of Kays et al. [3]**

Fig. 7 Comparison of models from literature with experimental results. Main-flow conditions $M_g = 2.1$, $T_{t,g} = 1039$–1060 K, and $P_{t,g} = 2.97$ bar.

$$B = \frac{h_{g,0}(T_{r,g} - T_{w,0})}{(T_{w,0} - T_{\mathrm{cu}})} \tag{12}$$

Using Eqs. (11) and (12) one can solve for the expected wall temperature T_w in the case of transpiration cooling:

$$T_w = \frac{aT_c + T_{r,g} + \frac{h_{g,0}}{h_g} T_{\mathrm{cu}} \frac{T_{r,g} - T_{w,0}}{T_{w,0} - T_{\mathrm{cu}}}}{1 + a + \frac{h_{g,0}}{h_g} \frac{T_{r,g} - T_{w,0}}{T_{w,0} - T_{\mathrm{cu}}}} \tag{13}$$

Here, a is a usually applied parameter describing the change in heat transfer toward the cooled wall, the effect of the specific heat capacity of the coolant $c_{p,c}$, and the blowing ratio F compared with the uncooled case:

$$a = \frac{F}{St_{g,0}} \frac{c_{p,c}}{c_{p,g}} \frac{St_{g,0}}{St_g} \tag{14}$$

For $St_g/St_{g,0}$ the model approach after Kays et al. [3] for a transpired boundary layer with foreign gas injection was used:

$$\frac{St_g}{St_{g,0}} = \frac{b_h}{e^{b_h} - 1} \qquad b_h = \frac{F}{St_{g,0}} \left(\frac{c_{p,c}}{c_{p,g}}\right)^{0.6} \qquad St_{g,0} = \frac{h_{g,0}}{\rho_g u_g c_{p,g}} \tag{15}$$

The hot-gas heat transfer coefficient $h_{g,0}$ or Stanton number $St_{g,0}$ are the only parameters left, which are unknown at this point. All other values can either be measured or obtained from tables. The hot-gas Stanton number can be estimated for our setup using the equation of Dittus and Boelter [43] for turbulent channel flow with the hydraulic diameter d as a reference length. Additionally, the correlation has been corrected for the not-fully-developed part up to the position where the sample is installed l:

$$St_{g,0} = 0.024 Re_d^{-0.2} Pr^{-0.7} \left[1 + \left(\frac{d}{l}\right)^{\frac{2}{3}}\right] \tag{16}$$

Using Eq. (16) leads to $St_{g,0} = 0.0034$ for our typical test conditions. Knowing the main-flow parameters and the properties of the coolants (see Table 4), we can solve for T_w from Eq. (13) and obtain a prediction of the porous-wall temperature. With this value, we can calculate the cooling efficiency as used and compare it with the measured values:

$$\Theta = \frac{T_{w,F=0} - T_w}{T_{w,F=0} - T_c} \tag{17}$$

where T_w is from the model calculation and the other temperatures are still from the measurements.

These data have been compared with the experimental results in Fig. 8. Within the margin of errors it is possible to predict the cooling efficiency of C/C within our test setup using a reasonable value for $St_{g,0}$. The influence of the different coolants can be captured quite well. This also shows that the approach of Kays et al. [3] predicts the

Table 4 Parameters for modified Kays et al. [3] model with heat conduction

Name	Symbol	Value
Hot-gas Mach number (measured)	M	2.06
Hot-gas total temperature (measured)	$T_{t,g}$	1039–1120 K
Hot-gas static pressure (measured)	$p_{s,g}$	0.346 bar
Stanton number without blowing (estimated)	$St_{g,0}$	0.0034
Porous-wall temperature without blowing (measured)	$T_{w,0}$	644 K
Copper temperature (measured)	T_{cu}	317 K
Specific heat capacity hot-gas	$c_{p,g}$	1024 J/(kg K)
Specific heat capacity coolant: air	$c_{p,c}$	1010 J/(kg K)
Specific heat capacity coolant: Ar	$c_{p,c}$	525 J/(kg K)
Specific heat capacity coolant: He	$c_{p,c}$	5193 J/(kg K)
Coolant temperature (measured) $f(F)$	T_c	309–395 K
Hot-gas bulk velocity	u_g	979–989 m/s
Hot-gas density	ρ_g	0.210–0.214 kg/m^3
Reynolds number	Re_d	269737–276293
Prandtl number	Pr	0.686

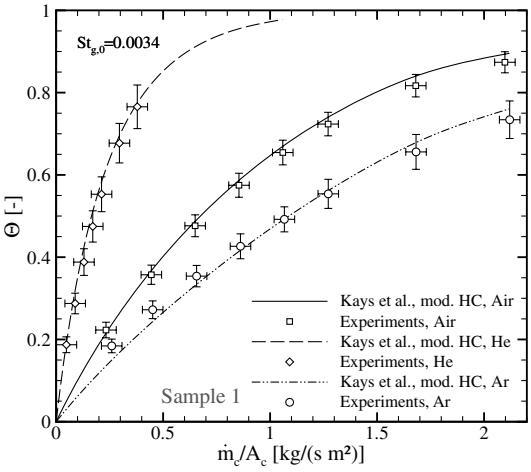

Fig. 8 Lateral heat conduction modified approach of Kays et al. [3] ($M_g = 2.1$, $T_{t,g} = 1039$–1060 K, and $p_{t,g} = 2.97$ bar); comparison with experimental results with different coolants.

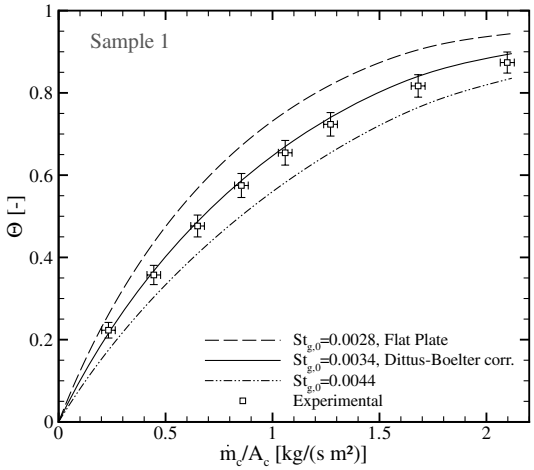

Fig. 9 Lateral heat conduction modified approach of Kays et al. [3] ($M_g = 2.1$, $T_{t,g} = 1060$ K, $p_{t,g} = 2.97$ bar, and air as coolant); effect of the variation of the hot-gas-side heat transfer coefficient without cooling $h_{g,0}$.

transpiration-cooling mechanisms very well, with respect to foreign gas injection. Generally, this approach is also valid for higher test temperatures appearing in real engine applications, but then the physics of reacting flows or real gas effects, for example, have to be taken into account when determining the heat transfer coefficient $h_{g,0}$.

The sensitivity of the model toward the channel heat transfer without blowing is shown in Fig. 9. The originally assumed Stanton number of 0.0044 over estimated the hot-gas-side heat transfer of about 29% and a Stanton number from a flat-plate correlation [see Eq. (18), which is about 18% lower than the modified Dittus and Boelter's [43] correlation] have been compared:

$$St_{g,0} = 0.037 Re_x^{-0.2} Pr^{-\frac{2}{3}} \tag{18}$$

The hot-gas-side heat transfer estimation has a nonnegligible effect on the cooling efficiency prediction. Altering $St_{0,g}$ in the margins given above, leads to a maximum error in the cooling efficiency of 23%, which appears at very low coolant mass-flow rates. For higher coolant mass-flow rates the impact of the heat transfer without blowing on Θ decreases.

D. Prediction of the Pressure Loss for Other Coolants Using the Wall-Temperature Model

For the model of the throughflow behavior of the C/C at higher test temperatures, a value of the wall temperature at a certain coolant mass-flow rate had to be given (Sec. IV.A) in order to obtain a value for the pressure drop. With the availability of the wall-temperature model developed in this study, this value can be provided for different coolants knowing the main-flow parameters and for given coolant mass-flow rates. First, the permeability coefficients for all test gases at ambient conditions without main flow were evaluated by a curve-fitting technique. These parameters are plotted in Fig. 10. The uncertainties in K_D and K_F were determined by a Monte Carlo method, which performed 10,000 curve fits using the uncertainties in the parameters $\mu_{in} v_{in}$ and $\rho_{in} v_{in}^2$ [see Eq. (2)] as a normal distributed input. The mean values, i.e., the values for the permeability coefficients obtained by applying this method, differ for the different test gases, due to the different coolant mass-flow rate regimes and the same test equipment used.

Nevertheless Fig. 10 shows, that within the margin of errors, all cold-flow tests yield similar permeability coefficients. This is because these parameters are material intrinsic values and should not depend on fluid properties or temperature. The high uncertainty of K_D and K_F for helium can be explained by the very low coolant mass-flow rates investigated with this gas. Using these coefficients and applying the throughflow model coupled with the wall-temperature model, one is able to compute the pressure drop for different coolants and conditions with thermal loads.

Figure 11a and 11b show these results compared with the experimental data with argon and helium for ambient and hot-gas conditions. The permeability coefficients were taken from the

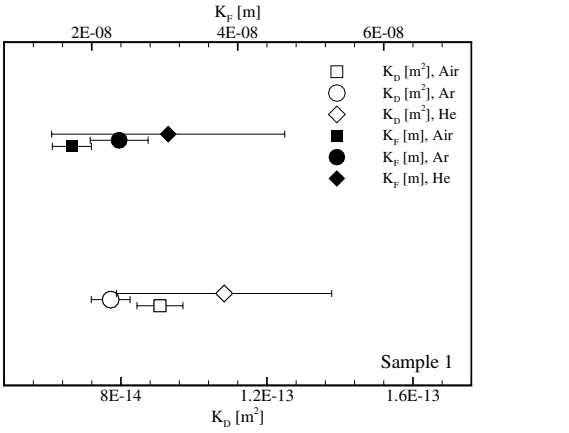

Fig. 10 Permeability coefficients K_D and K_F from the cold-flow tests for different coolants including uncertainties.

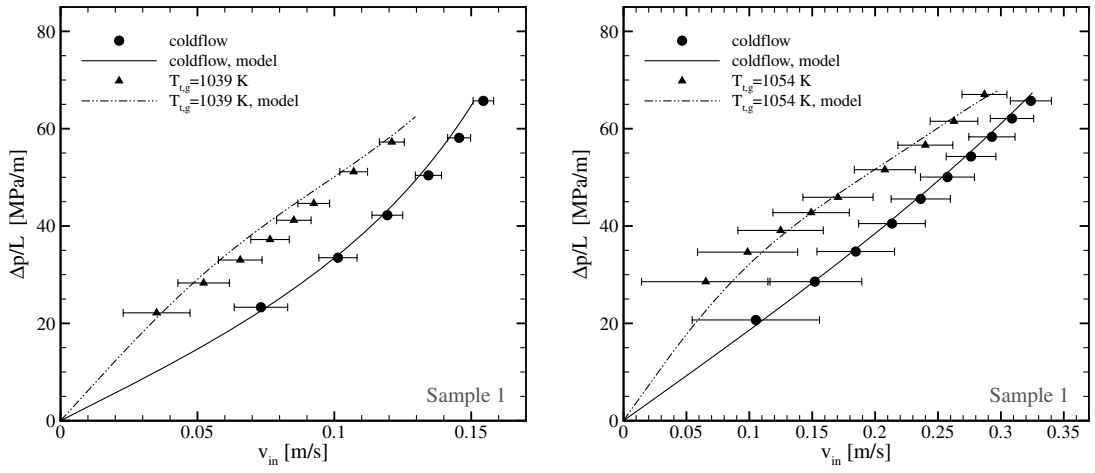

a) Coolant: Argon **b) Coolant: Helium**

Fig. 11 Normalized pressure loss versus superficial throughflow velocity: experimental data compared with coupled approach for the pressure loss using the cold-flow permeability coefficients.

throughflow tests at ambient temperature such as displayed in Fig. 10. To validate the developed model with the experimental results, the coefficients from the tests with the different test gases have been used. This ensures comparability with the measured pressure-loss data and allows the effect of nonisothermal coolants on the pressure drop to be examined for all gases used.

The agreement is very good meaning the effects of the nonisothermal porous wall can also be predicted well for different gases. This model can therefore be used to predict the pressure drop of a porous composite material for scramjet combustion-chamber application under thermal loading given the permeability coefficients from throughflow tests at ambient conditions without any hot-gas flow. These coefficients have to be determined accurately for the coolant to be applied using adequate test equipment to be able to obtain a good prediction of the real pressure loss. Additionally, the hot-gas-side Stanton number without blowing has to be known properly and the test or application specific conduction situations have to be addressed.

V. Conclusions

In this study, transpiration-cooling tests with $M = 2.1$ flow at total temperatures $T_{t,g}$ of up to 1120 K have been described using air, argon, and helium as coolants. Two-dimensional surface temperature maps of the C/C sample were recorded by IR thermography and calibrated with wall thermocouple measurements. From these data, the cooling efficiency Θ of the porous wall was presented. The main influencing parameters for Θ are the coolants' specific heat capacity and the coolant mass-flow rate. To validate this effect, a one-dimensional heat-balance model was developed, taking the lateral heat conduction within the experimental setup into account. This model showed good agreement with the experimental data. The approach of Kays et al. [3] was shown to adequately describe the transpiration-cooling effects for foreign gas injection if the test setup's specific thermal situation is taken into account. The developed model can be used for nonadiabatic high-temperature setups, which are common in aerospace propulsion applications or testing.

Furthermore, the pressure drop over the porous C/C wall was measured and the influence of the samples temperature distribution on the throughflow behavior was determined. Higher temperature levels within the porous wall lead to higher pressure drops. For this reason, the Darcy–Forchheimer equation was modified to capture this effect. The analytical data fit well to the measured pressure drop. With this analysis, it is possible to predict the pressure loss over a porous wall, for thermally loaded situations knowing the hot-gas-side wall temperature T_w for the different coolant mass-flow rates. This model was coupled to the transpiration-cooling model eliminating the wall temperature T_w. Now, the pressure drop of transpiration-cooled systems using porous CMCs can be estimated using the permeability coefficients of the porous wall evaluated from cold-flow experiments and the expected heat transfer without blowing for different coolant gases.

Acknowledgments

This work was performed within the ATLLAS (Aerodynamic and Thermal Load Interactions with Lightweight Advanced Materials for High-Speed Flight) project investigating high-speed transport. ATLLAS, coordinated by ESA's European Space Research and Technology Centre, is supported by the European Union within the 6th Framework Programme Priority 1.2, Aeronautic and Space, contract no. AST5-CT-2006-030729. Additional support by M. Kuhn and H. Hald of the DLR, German Aerospace Center, Institute of Structures and Design, and T. Cain of Gas Dynamics, Ltd., is greatly appreciated.

References

[1] Polezhaev, Y., "Will There or Will There Not Be a Hypersonic Airplane," *Journal of Engineering Physics and Thermophysics*, Vol. 73, No. 1, 2000, pp. 3–8. doi:10.1007/BF02681670

[2] Steelant, J., "Achievements obtained on Aero-Thermal Loaded Materials for High-Speed Atmospheric Vehicles within ATLLAS," 16th AIAA/DLR/DGLR International Space Planes and Hypersonic Systems and Technologies Conference, AIAA Paper 2009-7225, Bremen, Germany, 2009.

[3] Kays, W., Crawford, M., and Weigand, B., *Convective Heat and Mass Transfer*, 4th ed., McGraw–Hill, New York, 2005.

[4] Nield, D., and Bejan, A., *Convection in Porous Media*, 3rd ed., Springer, Berlin, 2006.

[5] Langener, T., Von Wolfersdorf, J., Cheuret, F., and Steelant, J., "Experimental and Numerical Study on Transpiration Cooling with Supersonic Flow," 19th ISABE Conf., ISABE Paper 2009-1238, Montreal, 2009.

[6] Cheuret, F., Steelant, J., Langener, T., and Von Wolfersdorf, J., "Simulations on Transpiration Cooling for Supersonic Flow," *Proceedings of the CEAS 2009, European Air and Space Conference*, CEAS, Manchester, UK, Oct. 2009.

[7] Rannie, W., "A Simplified Theory of Porous Wall Cooling," Tech. rep., Jet Propulsion Lab., Pasadena, CA, Nov. 1947.

[8] Eckert, E., and Livingood, J., "Comparison of Effectiveness of Convection-, Transpiration-, and Film-Cooling Methods with Air as Coolant," NACA, Lewis Flight Propulsion Lab. TR 1182, Cleveland, OH, 1954.

[9] Laganelli, A., "A Comparison Between Film Cooling and Transpiration Cooling System in High Speed Flow," *Proceedings of the AIAA 8th Aerospace Sciences Meeting*, AIAA Paper 1970-153, New York, NY, 1970.

[10] Rubesin, M., "An Analytical Estimation of the Effect of Transpiration Cooling on the Heat-Transfer and Skin-Friction Characteristics of a Compressible, Turbulent Boundary Layer," NACA Ames Aeronautical Labs., TN 3341, Moffett Field, CA, 1954.

[11] Mickley, H., Ross, R., Squyers, A., and Stewart, W., "Heat, Mass, and Momentum Transfer for Flow Over a Flat Plate with Blowing or Suction," NACA TN 3208,1954.

[12] Mickley, H. S., and Davis, R. S., "Momentum Transfer for Flow over a Flat Plate with Blowing," NACA TN 4017, 1957.

[13] Moffat, R., and Kays, W., "The Turbulent Boundary Layer on a Porous Plate: Experimental Heat Transfer with Uniform Blowing and Suction," *International Journal of Heat and Mass Transfer*, Vol. 11, 1968, pp. 1547–1566. doi:10.1016/0017-9310(68)90116-6

[14] Simpson, R., Moffat, R., and Kays, W., "The Turbulent Boundary Layer on a Porous Plate: Experimental Skin Friction with Variable Injection and Suction," *International Journal of Heat and Mass Transfer*, Vol. 12, No. 7, 1969, pp. 771–789. doi:10.1016/0017-9310(69)90181-1

[15] Herbertz, A., "Numerische Leistungsanalyse von Triebwerksauslegungen mit transpirativ gekühlter keramischer Raketenbrennkammer," *Proceedings of the DGLR Deutscher Luft- und Raumfahrtkongress*, DGLR, Munich, Germany, 2003.

[16] Greuel, D., Herbertz, A., Haidn, O., Ortelt, M., and Hald, H., "Transpiration Cooling Applied to C/C Liners of Cryogenic Liquid Rocket Engines," 40th AIAA/ASME/SAE/ASEE Joint Propulsion Conf. and Exhibit, AIAA Paper 2004-3682, Fort Lauderdale, FL, 2004.

[17] L'Ecuyer, M., and Colloday, R., "Influence of Porous-Wall Thermal Effectiveness on Turbulent-Boundary-Layer Heat Transfer," NASA TN D-6837, Lewis Research Center, Cleveland, OH, 1972.

[18] Chauvin, L., and Carter, H., "Exploratory Tests of Transpiration Cooling on a Porous 8° Cone at $M = 2.05$ Using Nitrogen Gas, Helium Gas, and Water as the Coolants," NACA RM L55C29, Langley Aeronautical Lab., Langley Field, VA, 1955.

[19] Bartle, E., and Leadon, M., "Experimental Evaluation of Heat Transfer With Transpiration Cooling in a Turbulent Boundary Layer at $M = 3.2$," *Journal of the Aerospace Sciences*, Vol. 26, 1959, pp. 78–80.

[20] Woodruff, L., and Lorenz, G., "Hypersonic Turbulent Transpiration Cooling Including Downstream Effects," *AIAA Journal*, Vol. 4, No. 7, 1966, pp. 969–975.

[21] Dorot, V., and Strelets, M., "Transpiration Cooling in a Supersonic Boundary Layer," *Teplofizika Vysokikh Temperatur*, Vol. 11, No. 3, 1973, pp. 64–68.

[22] Meinert, J., Huhn, J., Serbest, E., and Haidn, O., "Turbulent Boundary Layers with Foreign Gas Transpiration," *Journal of Spacecraft and Rockets*, Vol. 38, 2001, pp. 191–198. doi:10.2514/2.3693

[23] Serbest, E., "Untersuchungen zur Anwendung der Effusionskühlung bei Raketenbrennkammern," Ph.D. Thesis, RWTH Aachen, Germany, 2002.

[24] Krenkel, W., "Entwicklung Eines Kostengünstigen Verfahrens zur Herstellung von Bauteilen aus Keramischen Verbundwerkstoffen,"

German Aerospace Center (DLR), Stuttgart, Germany, 2000.
[25] Heidenreich, B., "Carbon Fibre Reinforced SiC Materials Based on Melt Infiltration," *Proceedings of the 6th International Conference on High Temperature Ceramic Matrix Composites*, New Delhi, India, 2007.
[26] Kelly, H., and Blosser, M., "Active Cooling From the Sixties to NASP," NASA Langley Research Center, TM-109079, Hampton, VA, 1994.
[27] Song, K., Choi, S., and Scotti, S., "Transpiration Cooling Experiment for Scramjet Engine Combustion Chamber by High Heat Fluxes," *Journal of Propulsion and Power*, Vol. 22, No. 1, 2006, pp. 96–102. doi:10.2514/1.11300
[28] Bouchez, M., and Beyer, S., "PTAH-SOCAR Fuel-Cooled Composite Material Structure," 15th AIAA International Space Planes and Hypersonic Systems and Technologies Conf., AIAA Paper 2008-2626, Dayton, OH, 2008.
[29] Serbest, E., Haidn, O., Hald, H., Korger, G., and Winkelmann, P., "Effusion Cooling in Rocket Combustors Applying Fiber Reinforced Ceramics," 35th AIAA/ASME/SAE/ASEE Joint Propulsion Conf. and Exhibit, AIAA Paper 1999-2911, Los Angeles, 1999.
[30] Hald, H., Ortelt, M., Fischer, I., Greuel, D., and Haidn, O., "Effusion Cooled CMC Rocket Combustion Chamber," AIAA/CIRA 13th International Space Planes and Hypersonics Systems and Technologies Conf., AIAA Paper 2005-3229, Capua, Italy, 2005.
[31] Langener, T., Von Wolfersdorf, J., Laux, T., and Steelant, J., "Experimental Investigation of Transpiration Cooling with Subsonic and Supersonic Flows at Moderate Temperature Levels," 44th AIAA/ASME/SAE/ASEE Joint Propulsion Conf. & Exhibit, AIAA Paper 2008-5174, Hartford, CT, 2008.
[32] Scheuermann, T., Chun, J., and Von Wolfersdorf, J., "Experimental Investigation of Scramjet Combustor Characteristics," 15th AIAA International Space Planes and Hypersonic Systems and Technologies Conf., AIAA Paper 2008-2552, Dayton, OH, 2008.
[33] Vellaramkalayil, J., Scheuermann, T., and Von Wolfersdorf, J., "Numerical and Experimental Investigation of a Two-Staged Supersonic Combustion Chamber," 16th AIAA/DLR/DGLR International Space Planes and Hypersonic Systems and Technologies Conf., AIAA Paper 2009-7363, Bremen, Germany, 2009.
[34] Martiny, M., Schiele, R., Gritsch, M., Schulz, A., and Wittig, S., "In Situ Calibration for Quantitative Infrared Thermography," *Proceedings of the Eurotherm Seminar No. 50*, Stuttgart, Germany, 1996.
[35] Schulz, A., "Infrared Thermography as Applied to Film Cooling of Gas Turbine Components," *Measurement Science and Technology*, Vol. 11, 2000, pp. 948–956. doi:10.1088/0957-0233/11/7/311
[36] Brauckmann, D., and Von Wolfersdorf, J., "Infrared Thermography with In-Situ Calibration Using Thermochromic Liquid Crystals Applied to Film Cooling," *Proceedings of ASME Turbo Expo 2004*, ASME, No. GT2004-53855, Vienna, 2004.
[37] Brauckmann, D., "Experimentelle Untersuchungen von Filmkühlungsvorgängen an Konturierten Bohrungen," Ph.D. Thesis, Univ. Stuttgart, Stuttgart, Germany, 2006.
[38] Kline, S., and McClintock, F., "Describing the Uncertainties in Single Sample Experiments," *Mechanical Engineering*, Vol. 1, 1953, pp. 3–8.
[39] Moffat, R., "Describing the Uncertainties in Experimental Results," *Experimental Thermal and Fluid Science*, Vol. 1, No. 1, 1988, pp. 3–17. doi:10.1016/0894-1777(88)90043-X
[40] Innocentini, M., Pardo, A., and Pandolfelli, V., "Modified Pressure-Decay Technique for Evaluating the Permeability of Highly Dense Refractories," *Journal of the American Ceramic Society*, Vol. 83, No. 1, 2000, pp. 220–222. doi:10.1111/j.1151-2916.2000.tb01175.x
[41] Moreira, E., Innocentini, M., and Coury, J., "Permeability of Ceramic Foams to Compressible and Incompressible Flow," *Journal of the European Ceramic Society*, Vol. 24, 2004, pp. 3209–3218. doi:10.1016/j.jeurceramsoc.2003.11.014
[42] REFPROP, Software Package, Ver. 8.0, *NIST Standard Reference Database 23*, National Institute of Standards and Technology, Gaithersburg, MD, 2007.
[43] Dittus, P. W., and Boelter, L. M. K., "Heat Transfer in Automobile Radiators of the Tubular Type," *International Communications in Heat and Mass Transfer*, Vol. 12, 1985, pp. 3–22. doi:10.1016/0735-1933(85)90003-X

K. Asai
Associate Editor